Research Article

Insight into the adsorption kinetics, mechanism, and thermodynamics of methylene blue from aqueous solution onto pectin-alginate-titania composite microparticles

Nur Izzah Iwanina Zamri[1] · Siti Lailatul N. Zulmajdi[1] · Nur Zafirah A. Daud[1] · Abdul Hanif Mahadi[2] · Eny Kusrini[3] · Anwar Usman[1]

Abstract
In the present study, pectin-alginate-titania (PAT) composites were synthesized and the adsorptive removal behavior of methylene blue (MB) from aqueous solution, as a model of synthetic organic effluents, onto the prepared PAT composites were investigated by monitoring the effect of contact time, initial MB concentration, and temperature. The adsorption isotherm data were fitted well with the Freundlich isotherm model, suggesting the surface heterogeneity of the PAT composites and that the MB adsorption occurred on the active sites on multilayer surface of the composites. The adsorption kinetics of MB was demonstrated to be pseudo-second order, governed by two intraparticle diffusion rates, and the adsorption process was exothermic, spontaneous, and more disorder. The Langmuir isotherm model suggested that the maximum adsorption capacity of MB on the PAT composites was in the range of 435–637 mg g^{-1}. In general, it increased with the TiO_2 NPs content in the PAT composites, due most likely to the increase in surface area exposing more functional groups of the pectin and alginate to interact with the synthetic dye. The adsorptive removal of MB by the PAT composites was found to be more efficient compared with many other reported adsorbents, such as graphene oxide hybrids, pectin microspheres, magnetite-silica-pectin composites, clay-based materials, chemically treated minerals, and agricultural waste. The present study therefore demonstrated for the first time that PAT composites are not only promising to be utilized as an adsorbent in wastewater treatment, but also provide an insight into the adsorption mechanism of the synthetic dyes onto the biopolymers-titania composites.

Graphic abstract Insight into the adsorption kinetics, mechanism, and thermodynamics of methylene blue from aqueous solution onto pectin-alginate-titania composite microparticles.

✉ Anwar Usman, anwar.usman@ubd.edu.bn | [1]Department of Chemistry, Faculty of Science, Universiti Brunei Darussalam, Jalan Tungku Link, Gadong BE1410, Brunei Darussalam. [2]Centre for Advanced Material and Energy Sciences, Universiti Brunei Darussalam, Jalan Tungku Link, Gadong BE1410, Brunei Darussalam. [3]Department of Chemical Engineering, Faculty of Engineering, Universitas Indonesia, Kampus Baru UI, Depok 16424, Indonesia.
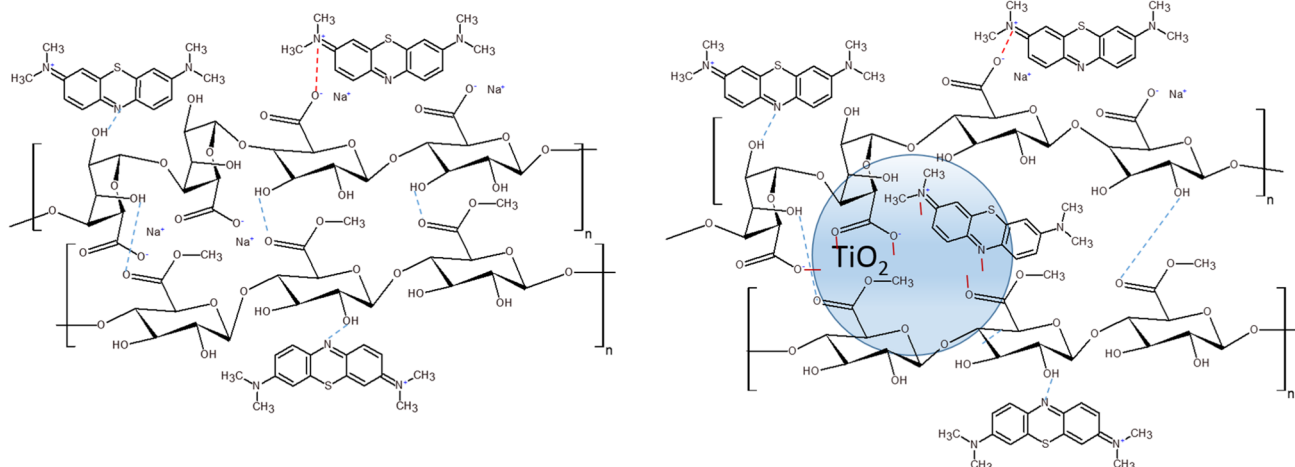
1 Introduction

Synthetic dyes are cost-effective and applicable for multiple purposes, therefore they have been utilized on a massive scale in textile, pulp, paper, pharmaceutical, and tannery industries [1]. Since most of the synthetic dyes, detergents, catalytic chemicals, and stabilizing agents are toxic, carcinogenic, mutagenic, or teratogenic to various living microorganisms, the industrial wastewater containing even low concentrations of dyes are dangerous to aquatic life in water systems [2–5]. In particular, if such the water systems are directly used as the sources of drinking water, the dye effluents can induce chronic diseases to major organs such as liver, brain, kidney, reproductive, and central nerve of humans [6, 7]. The synthetic dyes are well soluble and highly stable under ambient conditions and sunlight irradiation, thus it is indispensable to develop an efficient method to remove them from industrial wastewater to prevent the water systems from their contamination.

Various conventional chemical, physical, and biological methods have been demonstrated to be able to remove toxic pollutants, but their operation cost, removal efficiency, and generation of secondary pollutants still remain the main issues [8–11]. Amongst all the efficient removal methods, adsorption has attracted much attention due to its simple technical procedure, high removal rate, and regeneration of adsorbent [12–15]. In this regard, different types of materials have been explored as potential adsorbents [16–18], but the efficient adsorbent in focus is still centered on activated carbon because of its capability to adsorb different types of adsorbates [19]. Because of the expensive production and regeneration processes

of activated carbon, new types of adsorbents, including biopolymer- and polymer-based composites [20–26], and chemically modified agricultural waste materials [16, 27–29] have been explored. The other method of interest is the use of advanced oxidation processes, especially using titanium oxide nanoparticles (TiO$_2$ NPs) as a photocatalyst to generate solvated oxygen-based radicals capable to oxidize the synthetic dyes in water solution [30, 31]. However, the efficiency of the photo-induced degradation of the synthetic dyes is generally very low due to the electron–hole recombination and the low adsorptive capability of the photocatalyst [32–35]. Coupling the photocatalyst with a polymer in nanocomposites has been proven to be able to suppress the recombination process, improving the photodegradation efficiency of TiO$_2$ NPs [36]. On the other hand, the incorporation of the TiO$_2$ NPs into the biopolymers matrices in the chitosan-based composites has been demonstrated to enhance the adsorption capacity of the synthetic dyes [21, 23].

The present study was, therefore, mainly focused on the adsorptive removal of methylene blue (MB) on TiO$_2$-loaded pectin-alginate (PAT) composites. The objective is to explore the effect of incorporation of TiO$_2$ NPs into the crosslinked pectin-alginate matrix, aiming on the efficient PAT composite as a promising adsorbent for the removal of the synthetic dye from wastewater. To this purpose, the PAT composites with different loading contents of TiO$_2$ NPs were prepared using the precipitation method, and they were characterized using spectroscopic and imaging methods. MB was particularly selected in this study because it is one of azo dyes, which is a major class of synthetic dyes most commonly used in the textile industry

for dyeing cotton, wool, and silk, and effluent discharge containing MB has been environmental concerns due to its intense color, carcinogenic, or mutagenic properties [6, 37, 38]. The adsorptive removal of MB using the PAT composites was investigated in the batch system across different parameters, including contact time, initial dye concentration, temperature, and loading content of TiO_2 NPs. Finally, the adsorption behavior, e.g. adsorption capacity, mechanism, kinetics, isotherm, and thermodynamics of MB onto the PAT composites with different TiO_2 NPs loading contents were evaluated and established.

2 Materials and methods

2.1 Chemicals and reagents

The analytical grade methylene blue (MB) (CAS: 61-73-4) used in this work was purchased from Unilab. Commercially available anatase TiO_2 NPs (CAS: 13463-67-7) with 100 nm in size and alginic acid sodium salt (Na-Alg) (CAS: 9005-38-3) extracted from brown algae were obtained from Sigma-Aldrich and Fluka, respectively. These chemicals were used as received without any further purifications. Pectin used in this study was extracted from pomelo (*Citrus maxima*) pith in our laboratory, and the detailed extraction procedure has been previously reported [39]. Double distilled water was used throughout experiments.

2.2 Preparation of PAT composites

The PAT composites were prepared according to the protocol reported by Biswal et al. [40] with slight modifications. Pectin (1.0 g) and Na-alginate (1.0 g) were mixed with various amounts of TiO_2 NPs (0, 0.01, 0.10, and 0.50 g) in 50 mL distilled water, and the mixture was stirred for 15 min, followed by vacuum filtration. The filtrate was then dried in an oven at 70–80 °C, ground, and sieved using 212-μm mesh. The composites with different loading contents of TiO_2 NPs were labeled as $PAT^{(0)}$, $PAT^{(0.005)}$, $PAT^{(0.05)}$, and $PAT^{(0.25)}$ according to the weight percentage of the TiO_2 NPs in the mixture. The dried composites were carefully stored in zipped plastic bags and put in a desiccator before further use for characterizations and adsorption experiments.

2.3 Characterization of PAT composites

The functional groups of PAT composites which involved in the removal of synthetic dyes were identified based on the vibrational spectra of the adsorbent before and after MB adsorption measured using Fourier transform infrared (FTIR) spectrometer (IR Prestise-21, Shimadzu). The

spectra were measured in the range of 400–4000 cm^{-1} with the resolution of 2.0 cm^{-1}. The surface morphology of the PAT composites was visualized by scanning electron microscopic (SEM) imaging on a microscope (JSM-7600F, JEOL) operating at 5.0 kV with a magnification of 20,000×. The Brunauer–Emmett–Teller (BET) surface area and Barrett-Joyner-Halenda (BJH) pore size distribution of the PAT composites were measured by a surface analyzer (ASAP 2460, Micromeritics) based on a multipoint adsorption–desorption method. The crystallinity of the PAT composites was determined using X-ray diffractometer (XRD-7000, Shimadzu) with Cu Kα radiation (λ = 0.15418 nm) operating at 30 mA and 40 kV. The XRD data were collected over the diffraction 2θ angle in the range of 10°–80° at a scan rate of 1.0° min^{-1}.

The net charge on the PAT surface was determined based on pH changes of the KNO_3 solution (20 mL, 0.1 mol L^{-1}) containing colloid of 200 mg of the composite. The initial pH (pH$_{initial}$) of the KNO_3 solution was set to be in the range of 2–12. The colloidal solutions were gently stirred for 24 h at 25 °C, decanted through filter paper to remove the particulates, and then subjected to the measurement of the final pH (pH$_{final}$). The difference pH which was calculated as $\Delta pH = pH_{final} – pH_{initial}$ was plotted against the pH$_{initial}$, and the point at which $\Delta pH = 0$ was considered as pH at the point of zero charge (pH$_{pzc}$).

2.4 Adsorptive removal of MB by PAT composites

The effect of contact time was initially evaluated by mixing 5.0 mg of each PAT composite and 10 mL aqueous solution of MB (10 mg L^{-1}) in thirteen conical flasks (25 mL). All the colloidal mixtures were shaken at room temperature (25 °C) using orbital shaker with a speed of 150 rpm. The conical flasks containing the mixtures were wrapped with aluminum foil in order to prevent interaction with stray light that can lead to any photolysis and photocatalysis. After the desired contact time, the mixture in one of the conical flasks was centrifuged at 3000 rpm for 15 min. The supernatant was then collected and its absorption spectrum in the range of 200–800 nm was measured using 1 cm quartz cuvette cell on a UV–visible spectrophotometer (UV-1900, Shimadzu). In this sense, the MB adsorption on the PAT composites was evaluated at certain time intervals until the saturation condition was achieved.

Similar to the abovementioned procedures, the effect of initial concentration (also known as adsorption isotherm data) was evaluated from the mixture of 10 mL MB solutions ranging from 5.0 to 30 mg L^{-1} and a constant mass of 5.0 mg PAT composites at 25 °C. In addition, the effect of temperature on the adsorption was deduced from the mixture of 10 mL MB solution (10 mg L^{-1}) and 5.0 mg PAT

composites at different temperatures between 25 and 50 °C.

The removal efficiency (η) and adsorption capacity (Q_t) of MB on the PAT composites were calculated using Eq. (1 and 2), respectively,

$$\eta(\%) = \frac{(C_0 - C_t)}{C_0} \times 100\% \tag{1}$$

$$Q_t = \frac{(C_0 - C_t)}{M} \times V \tag{2}$$

where C_0 and C_t (in mol L^{-1}) are the initial and remaining concentration of dyes in the solution after adsorption at the contact time t (in min), V (in L) is the volume of the MB solution, and M (in g) is the mass of the PAT composite in the mixture, respectively.

2.5 Adsorption kinetics

The adsorption kinetics of MB onto the PAT composites was evaluated using Lagergren pseudo-first order [41] and pseudo-second order [42] by fitting the Q_t data acquired empirically with Eq. (3) and (4), respectively;

$$ln(Q_e - Q_t) = \ln Q_e - k_1 t \tag{3}$$

$$t/Q_t = 1/k_2 Q_e^2 + t/Q_e \tag{4}$$

Here, Q_e denotes the adsorptive removal capacity of MB at equilibrium condition, k_1 and k_2 is the pseudo-first and pseudo-second order rate constant, respectively. In order to elucidate the diffusion behaviors, including external and internal diffusion, governing the adsorption of the synthetic dye, the Q_t data were evaluated using Weber-Morris intraparticle [43] and Boyd diffusion models [44] by fitting them with Eq. (5 and 6), respectively;

$$Q_t = k_i t^{1/2} + C \tag{5}$$

$$B_t = -0.4977 - \ln\left(1 - \frac{Q_t}{Q_e}\right) \tag{6}$$

where k_i represents the intraparticle diffusion rate constants, and B_t is Boyd constant related to the fraction of MB adsorbed on the PAT composites.

2.6 Adsorption isotherm and the effect of temperature

The initial concentration dependence on MB adsorption onto the PAT composites was analyzed using empirical equilibrium equations with two independent parameters; namely Langmuir, Freundlich, Temkin, and Dubinin–Radushkevich isotherm models [45]. In this sense, the adsorption

isotherm data were fitted with the respective linear equations of the isotherm models, as given by Eq. (7–10);

$$1/Q_e = 1/Q_m K_L \times 1/C_e + 1/Q_m \tag{7}$$

$$Log Q_e = \frac{1}{n} Log C_e + Log K_F \tag{8}$$

$$Q_e = \frac{RT}{b_T}\left(ln K_T + ln C_e\right) \tag{9}$$

$$\ln Q_e = \ln Q_m - \beta\left\{RT \ln\left(1 + \frac{1}{C_e}\right)\right\}^2 \tag{10}$$

where Q_m is the maximum adsorption capacity, K_L is the Langmuir equilibrium constant, K_F is the Freundlich adsorption isotherm constant, n is the Freundlich exponent, K_T and b_T are the Temkin isotherm constants, β is the mean free energy of the adsorption based on the Dubinin–Radushkevich model, R is gas constant, and T is absolute temperature.

The effect of temperature on the adsorption kinetics of MB was evaluated by calculating the dimensionless equilibrium constant (K_e^0) using Eq. (11) [46, 47];

$$K_e^0 = K_g \times [MB]/\gamma \tag{11}$$

where K_g (in L mol^{-1}) is the equilibrium constant of the best fit of Langmuir or Sips isotherm models on the experimental data, $[MB]$ (in mol L^{-1}) is the concentration of the adsorbate, and γ is the coefficient of activity of the adsorbate. In this study, a diluted MB solution with the concentration of 3.13×10^{-5} mol L^{-1} was used, and hence the coefficient activity of the adsorbate has been taken to be unitary [47]. The adsorption Gibbs free energy (ΔG_{ads}^0) was then calculated based on Van't Hoff equation (Eq. 12);

$$\Delta G_{ads}^0 = -RT ln K_e^0 \tag{12}$$

The changes in enthalpy and entropy (ΔH^o and ΔS^o) of the adsorption were estimated from the y-intercept and slope of the linear regression plot of ΔG_{ads}^0 as a function of T, respectively.

2.7 Data analysis

The adsorption experiments were repeated in triplicate. All obtained data were analyzed. The data analyses, plotting, and fitting were performed using Origin software.

3 Results and discussions

3.1 Characterization of PAT composites

Figure 1 shows the FTIR spectra of the prepared PAT composites before and after MB adsorption. Before MB adsorption, PAT[(0)] composite (panel a; upper graph) showed sharp intense spectral bands at 685, 789, 1073, 1133, 1263, 1408, 1629, and 1735 cm^{−1}. In the finger print region, the bands at 1073 and 1735 cm^{−1} approved the stretching vibrations
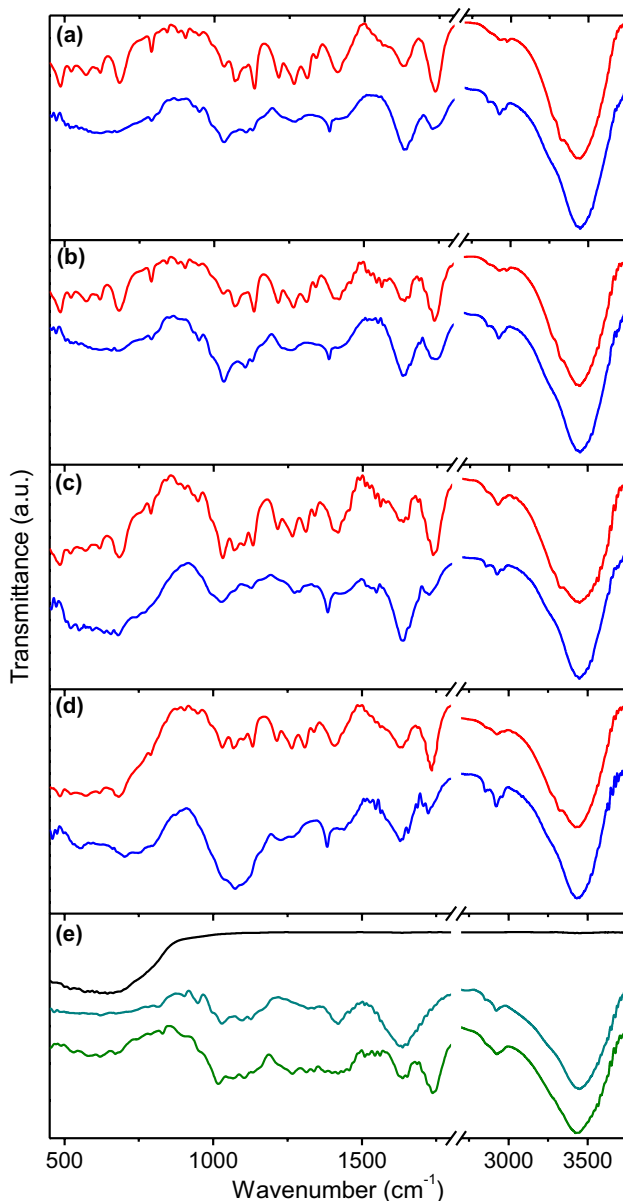

Fig. 1 FTIR spectra of **a** PAT[(0)] , **b** PAT[(0.005)], **c** PAT[(0.05)], **d** PAT[(0.25)] before (Red line) and after (Lite Blue line) MB adsorption, and **e** pectin (Dark Blue line), Na-alginate (Green line), and TiO$_2$ NPs (Black line).

of C−O and the carbonyl (C=O) of pectin and alginate [48, 49], whereas the peaks at 1408 and 1629 cm^{−1} can be attributed to the asymmetric and symmetric stretching modes of the carboxylic (COOH) group of pectin, respectively. The band at 1263 cm^{−1} is assigned to C−H bending vibration of pyranose ring [50], and the band at 1133 cm^{−1} may represent the −C−O−C glycosidic ring vibrations of pectin and alginate [51]. The FTIR spectrum of PAT[(0)] also shows a broad band between 3031 and 3793 cm^{−1}, denoting the O−H stretching of hydroxyl (−OH) group in the polysaccharides. Upon comparing the FTIR spectrum of PAT[(0)] with those of pectin and alginate (panel e), it is clearly observed that the FTIR spectrum of PAT[(0)] resembles the sum of the spectra of pectin and alginate [40]. Thus, one might consider that the two biopolymers in PAT[(0)] are interconnected through hydrogen bonds without changing their chemical structures. Similar spectral feature was observed in the FTIR spectra of PAT[(0.005)], PAT[(0.05)], and PAT[(0.25)] (panels b–d; upper graph), although the intensity of broad band at 600 cm^{−1} originated from the TiO$_2$ NPs increases continuously with their incorporation into the composites. It is noteworthy that the frequency of O−H vibrational band of pectin and alginate was slightly up-shifted from 3436 to 3444 cm^{−1}, suggesting that the vibration of OH groups of the two biopolymers are slightly affected upon the incorporation of TiO$_2$ NPs. Overall, the FTIR spectra suggested that the chemical structures of pectin and alginate remained intact, and the biopolymers might interact with the Ti atoms on the surface of the NPs, as illustrated in Fig. 2a.

Upon MB adsorption, a sharp band is clearly observed at 1381 cm^{−1} (see panels a–d; lower graphs) which is originated from the adsorbed MB onto the PAT composites. The relative peak intensity of the C−O, C=O, and −COO⁻ groups of PAT composite are modified, though their peak positions remain unchanged. In contrast, the peak position and intensity of the O−H vibrational band are almost unchanged, indicating that this functional group is not affected in the adsorption process. Overall, the results indicate that the MB adsorption took place mainly via weak interactions between the synthetic dye with the C−O, C=O, and COO⁻ functional groups of pectin and alginate in the PAT composites. It is noteworthy that the intensity of the broad band with the peak at 1077 cm^{−1} increases with the TiO$_2$ NPs contents in the PAT composites. In this sense, the interaction between the electron-deficient heterocyclic ring of MB and electron-rich Ti atoms on the surface of TiO$_2$ NPs is also considered. Overall, the spectral change indicates that the MB adsorption is mainly due to the dipole−dipole hydrogen-bonding interactions involving the −O−H, C=O, and −C−O bonds of the PAT composites and electrostatic interaction between the positively charged synthetic dye and the negatively
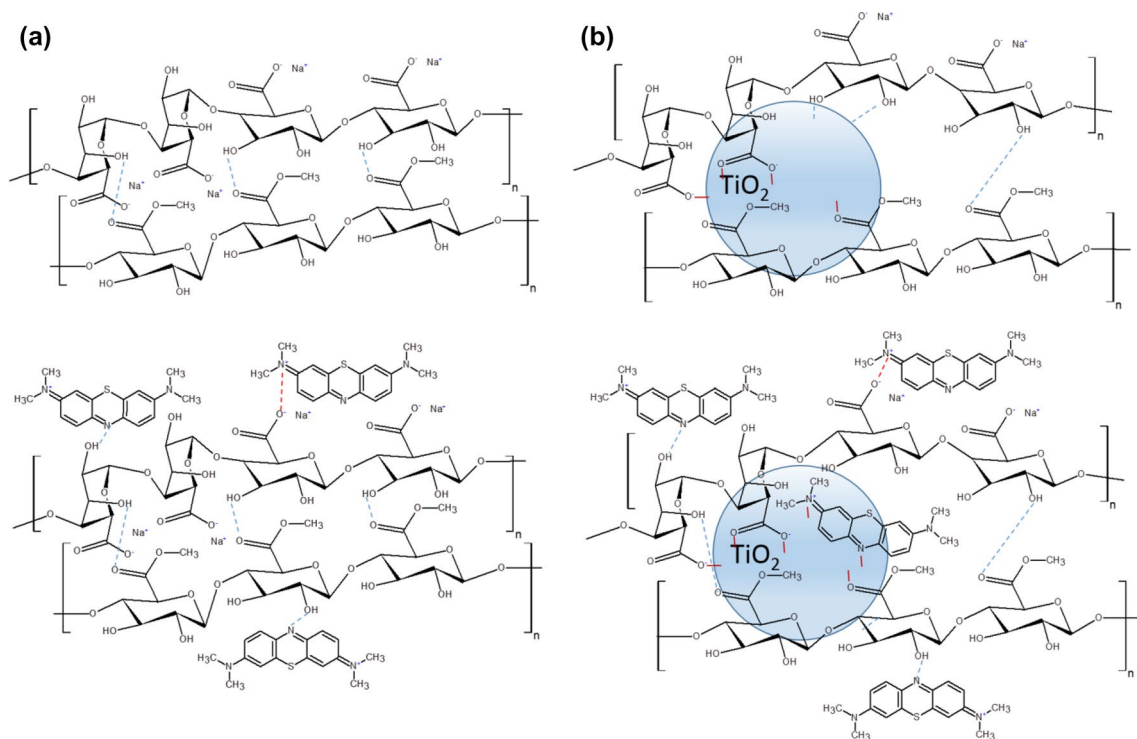
Fig. 2 Schematic illustrations of chemical structures of Pec and Alg based on FTIR spectra; **a** in the absence and **b** in the presence of incorporated of TiO_2 NPs before (upper graphs) and after (lower graphs) MB adsorption, depicting the possible adsorption mechanisms of MB onto the PAT composites. The electrostatic attractions, hydrogen bonding, and intermolecular interactions with the Ti atoms on the surface of TiO_2 NPs are denoted by blue dashed lines, dashed lines, and solid red lines, respectively

charged carboxylate ($-COO^-$) group on the surface of the composites, as schematically illustrated in Fig. 2b.

SEM images of the PAT composites with different loading contents of TiO_2 NPs before and after MB adsorption are shown in Fig. 3. The images indicated that pectin and alginate were blended and agglomerated into irregular and rough surface microparticles (panel a). The surface roughness of PAT composites increased with TiO_2 NPs content (panels b–d), due probably to the modification of intermolecular interactions between pectin and alginate upon incorporation of TiO_2 NPs, as suggested by the FTIR spectra. Upon MB adsorption, SEM images suggested that the surface of all the PAT composites became
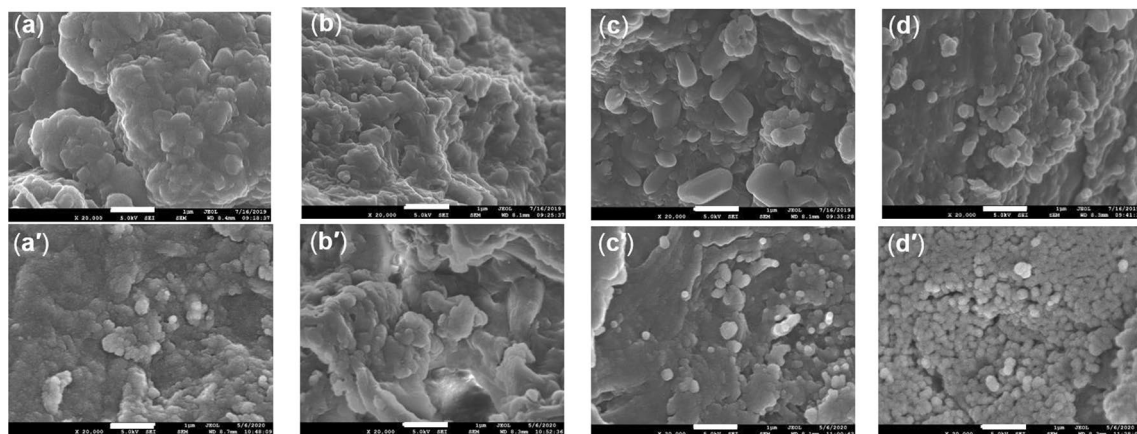

Fig. 3 Scanning electron micrographs of **a;a'** PAT$^{(0)}$, **b;b'** PAT$^{(0.005)}$, **c;c'** PAT$^{(0.05)}$, and **d;d'** PAT$^{(0.25)}$ before and after MB adsorption. The SEM image magnification was 20,000×, and the scale bars represent a 1-µm size

rougher, and the roughness increased with the TiO_2 NPs loading content (see panels a'–d').

The BET surface area of the PAT composites was found to increase from 2.31 to 13.5 m^2 g^{-1}, while the BJH pore size enhanced from 0.008 to 0.053 cm^3 g^{-1} with the TiO_2 NPs loading content, supporting the notion that the surface roughness was increased with TiO_2 NPs content. The role of the surface area and pore size in the adsorptive removal of MB will be described in more detail in Sect. 3.6.

The pH_{pzc} of PAT composites with different loading contents of TiO_2 NPs was found to be 4.27–4.48 as shown in Fig. 4. This suggested that the PAT composites have a negatively net surface charge at ambient pH. The negative net surface charge of PAT composites might be attributed to the large number of carboxylic acid functional groups (pKa 4–5) originated from the pectin and alginate which turn into carboxylate anions at ambient pH. It is noteworthy that the incorporation of TiO_2 NPs did not change the surface charge but it modified the structure and increased the surface area of the PAT composites.

The crystalline properties and the incorporation of TiO_2 NPs into the PAT composites were characterized using XRD analysis, and the results are shown in Fig. 5. PAT[(0)] composite (panel a) showed mainly a broad band at $2\theta = 20°–50°$ due to amorphous phase of pectin and alginate (see Fig. S1 in Supplementary Information) [52, 53]. Upon incorporation of TiO_2 NPs, the crystallinity of the PAT composites was increased (panels a–d). The diffraction peaks of TiO_2 NPs in the PAT composites were clearly observed at 25.3°, 37.7°, 47.9°, 53.9°, 54.9°, 62.6°, 68.9°, 70.3° and 75.1°, as demonstrated by PAT[(0.05)] and PAT[(0.25)] (panels c, d). These diffraction peaks have been assigned to (101), (004), (200), (105), (211), (204), (116),
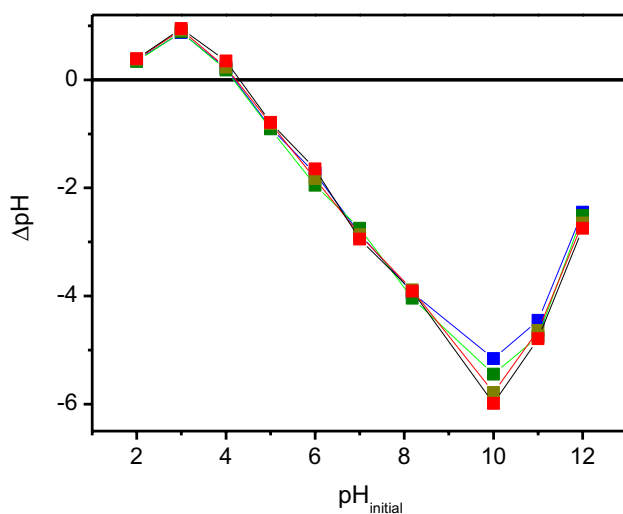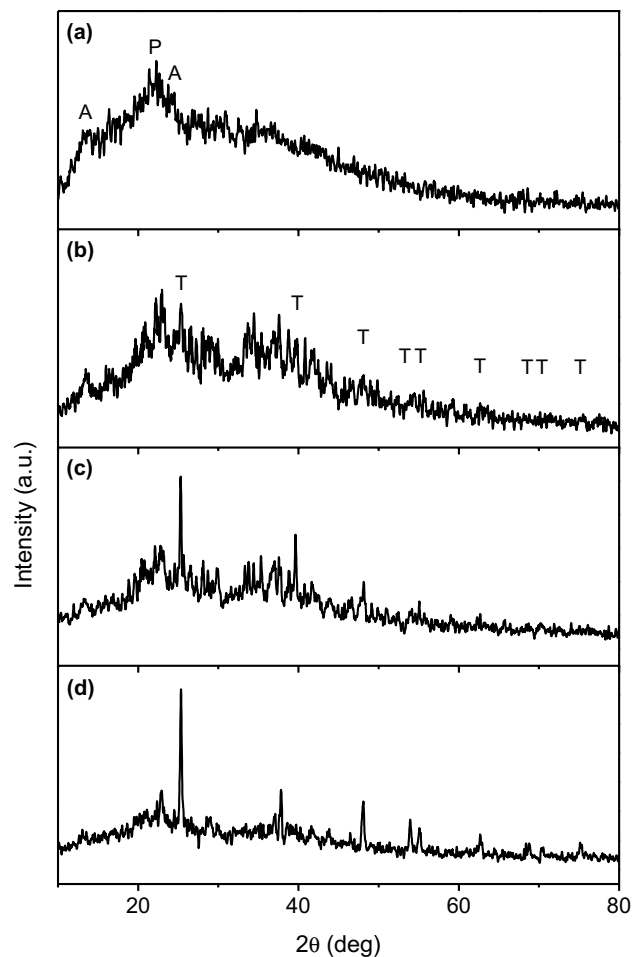

Fig. 5 XRD patterns of **a** PAT[(0)], **b** PAT[(0.005)], **c** PAT[(0.05)], and **d** PAT[(0.25)]. P, A, and T denote the diffraction peaks of Pec, Alg, and TiO_2 NPs

(220), and (215) planes of crystalline anatase phase of TiO_2 NPs [54]. By comparing the XRD patterns of PAT composites and TiO_2 NPs (see Fig. S2), the crystalline phase and particle size of TiO_2 NPs incorporated in the pectin-alginate matrix in the PAT composites remained unchanged.

3.2 MB adsorption on the PAT composites

The MB adsorption onto the PAT composites from their colloidal mixtures is reflected by the decrease in absorption intensity of MB solution, as shown in Fig. 6 for PAT[(0)] and PAT[(0.005)] (as representative examples). Based on the absorption intensity change, the plot of η value against the contact time, t, is shown in Fig. S3a, suggesting that MB adsorption on the PAT composites was saturated at the contact time longer than 15 min. The η values of MB adsorption from the mixture of 5.0 mg of the PAT[(0)] or PAT[(0.005)] with 10 mL solution of MB (10 mg L^{-1}), at the equilibrium condition at the contact time of 30 min, were
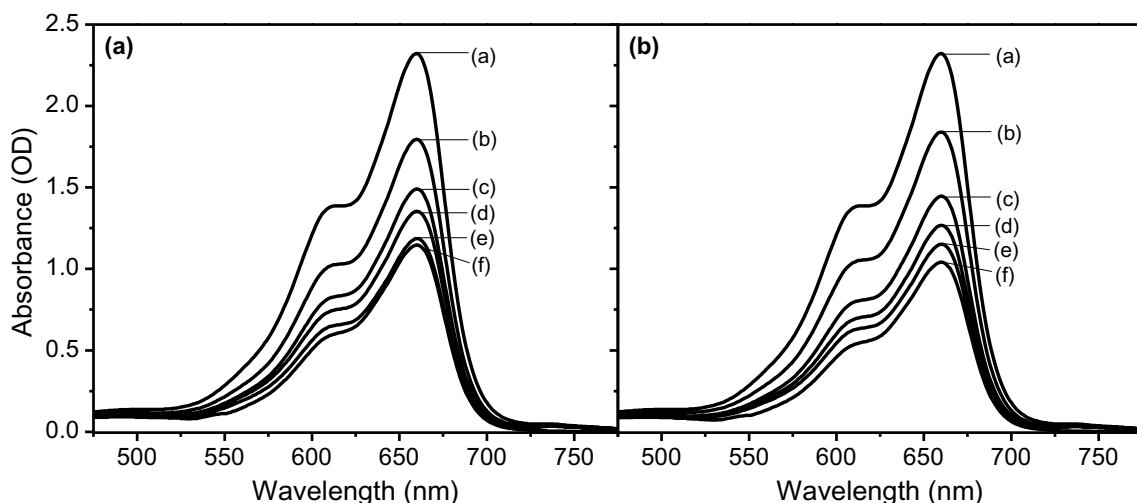

Fig. 4 Point of zero charge (pH_{PZC}) of PAT[(0)] (Red square), PAT[(0.005)] (Lite Green square), PAT[(0.05)] (Dark Green square), PAT[(0.25)] (Blue square)

Fig. 6 Time evolution of absorption spectra of 10 mg L^{-1} MB upon adsorption on **a** PAT$^{(0)}$ and **b** PAT$^{(0.005)}$ composites after the contact time of (**a**) 0, (**b**) 1, (**c**) 5, (**d**) 10, (**e**) 15, and (**f**) 30 min

51 and 56%. The Q_t values of the same mixture are shown in Fig. 7a, where the experimental equilibrium adsorption capacity (Q_e) of MB adsorption on PAT$^{(0)}$ and PAT$^{(0.005)}$ was estimated to be 13.9 and 15.3 mg g^{-1}, respectively. With the same experimental conditions, the increase in the initial MB concentration led to the decrease in the η value (see Fig. S3b), as more dyes in the solution remained in the solution, whereas the Q_e values increased nonlinearly with the equilibrium concentration (C_e) of MB, as shown in Fig. 7b. This adsorption isotherm data will be analyzed and elucidated in detail in the next section.

The adsorption kinetics data of MB on PAT$^{(0)}$ and PAT$^{(0.005)}$ were analyzed using Lagergren pseudo-first order and pseudo-second order, as shown in Fig. 8a, b,

and the adsorption kinetics parameters of the two kinetics models are summarized in Table 1. The best fit of the linear equations suggested that the pseudo-second order kinetics model gave the $Q_{e,calc}$ values close to the experimental Q_e values. Moreover, the regression coefficient (R^2) for the pseudo-second order kinetics model was 0.994 and 0.998 for the MB absorption on PAT$^{(0)}$ and PAT$^{(0.005)}$, respectively, better than the Lagergren pseudo-first order kinetic model. This finding suggested that the adsorption kinetics of MB on both PAT$^{(0)}$ and PAT$^{(0.005)}$ was pseudo-second order. With its pseudo-second order kinetics, the MB adsorption could be categorized as a chemisorption [55], involving its electrostatic and hydrogen bonding interactions with functional groups on the surface of the
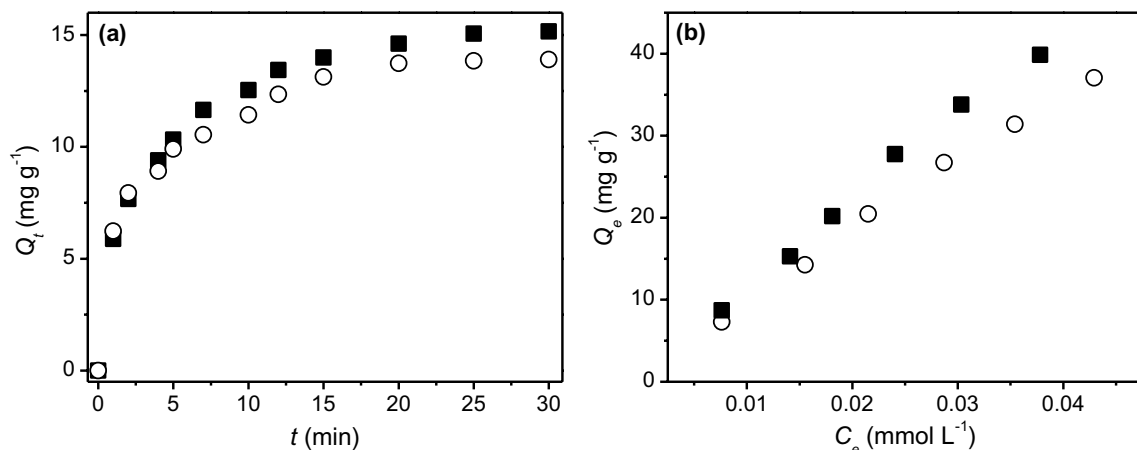

Fig. 7 The plots of **a** the adsorption capacity (Q_t) of MB on PAT$^{(0)}$ (Circle) and on PAT$^{(0.005)}$ (Filled square) against the contact time, t, for the intial MB concentration of 3.13×10^{-5} mol L^{-1}, and **b** the equilibrium adsorption capacity (Q_e) as a function of the equilibrium concentration (C_e) of MB
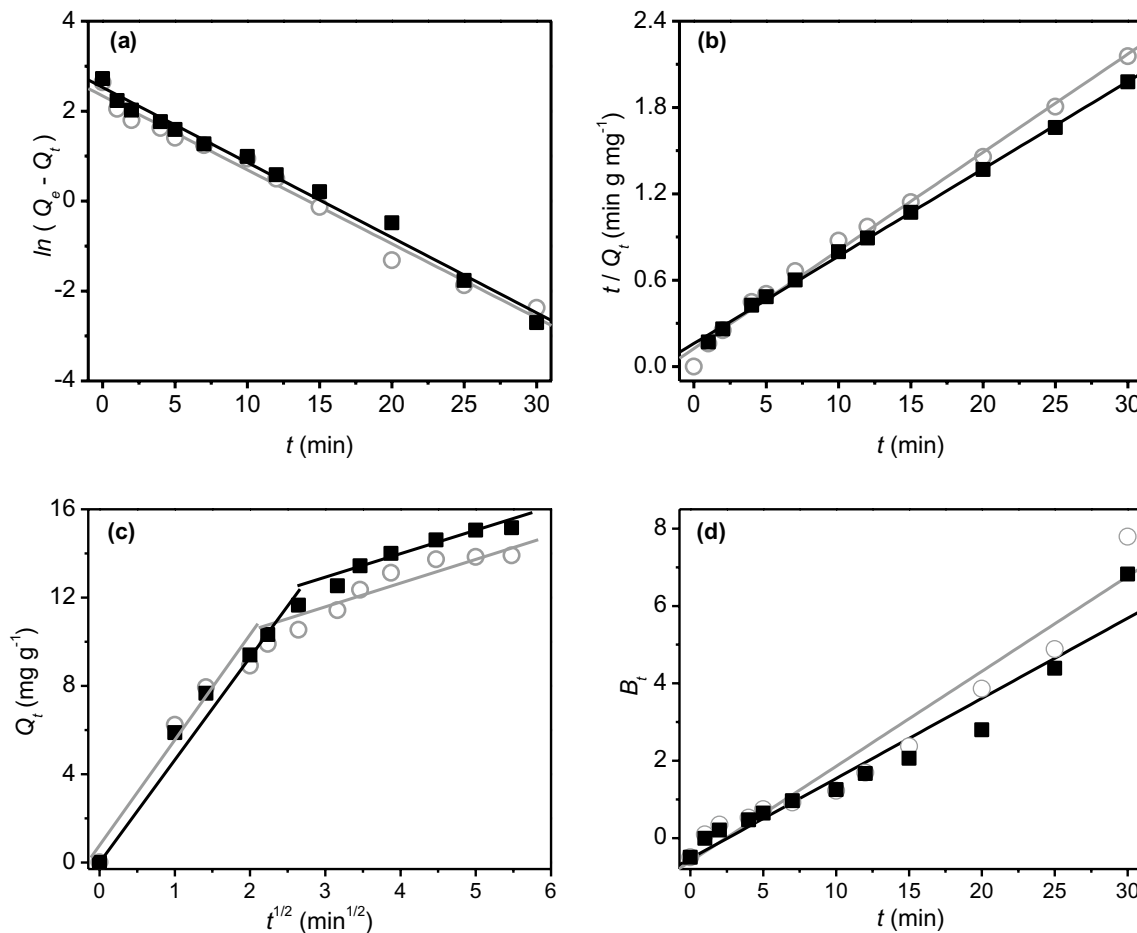
Fig. 8 The adsorption kinetic data of MB on PAT[(0)] (Circle) and PAT[(0.005)] (Filled circle) fitted with **a** Lagergren pseudo-first order, **b** pseudo-second order, **c** Weber-Morris intraparticle diffusion, and **d** Boyd diffusion models. The grey and black solid lines are the best fits of MB adsorption data on PAT[(0)] and PAT[(0.005)]

Table 1 The adsorption kinetics parameters of MB on PAT[(0)] and PAT[(0.005)] calculated from the best fitting of Lagergren pseudo-first order and pseudo-second order kinetics models on the experimental data

Kinetics model	Parameters	PAT[(0)]	PAT[(0.005)]
Lagergren pseudo-first order			
	$Q_{e,calc}$ (mg g^{-1})	10.4	12.5
	k_1 (min^{-1})	0.164	0.167
	R^2	0.985	0.989
	χ^2	0.044	0.034
Pseudo-second order			
	$Q_{e,calc}$ (mg g^{-1})	14.7	16.5
	k_2 (g mg^{-1} min^{-1})	0.037	0.023
	R^2	0.994	0.998
	χ^2	0.003	< 0.001

PAT composites. Similar adsorption kinetics of MB onto agricultural waste based adsorbents has also been generally observed [56].

The time-dependent MB adsorption was also evaluated using Weber-Morris intraparticle and Boyd diffusion models. Fitting the experimental data with the Weber-Morris intraparticle model suggested two diffusion behaviors (Fig. 8c); where the fast intraparticle diffusion phase took place within early 5–10 min of contact time with k_i being 4.68 and 5.14 mg g^{-1} min$^{-1/2}$ for the MB adsorption on PAT[(0)] and PAT[(0.005)], respectively, followed by a slower diffusion at longer contact time with k_i being 1.00–1.10 mg g^{-1} min$^{-1/2}$ associated with the equilibrium phase. The y-intercept of the best fit of the intraparticle diffusion model was close to zero, indicating that the MB adsorption on the PAT composites was diffusion rate-limiting process. This notion was supported by fitting the data with the Boyd diffusion model (Fig. 8d). However, the model line does not pass exactly through the origin and all the data point. Based on Boyd's criterion [44, 57], these findings suggested that the diffusion rate-limiting process of adsorption was the external mass transport attributed to both the intraparticle and film diffusion [58].

3.3 Adsorption isotherm

The adsorption isotherm data of MB on the PAT composites were evaluated using various empirical Langmuir, Freundlich, Temkin, and Dubinin–Radushkevich isotherm models. As shown in Fig. 9a–d for PAT$^{(0)}$ and PAT$^{(0.005)}$ as representative examples of adsorbents, the Q_e values of different MB concentrations were fitted with the four isotherm models using Eq. (7–10), respectively. The R^2 and χ^2 values of the fitting simulations along with all the fitting parameters of the adsorption isotherm data are summarized in Table 2. Among the four different isotherm models applied in this study, the simulation plots of Langmuir and Freundlich models closely passed through the experimental data (Fig. 9a, b), whereas those of Temkin and Dubinin–Radushkevich models were deviated (Fig. 9c, d) and they could be therefore obviously ruled out. Although the simulation plots of Langmuir and Freundlich models gave the same R^2 values, but χ^2 value of Freundlich isotherm is lower than Langmuir model. This finding suggested that the adsorption mechanism of MB onto the PAT

composites followed Freundlich isotherm model, implying the surface heterogeneity of the PAT composites. Taken the basic hypothesis of Freundlich isotherm model into account, the adsorption process of MB should occur on active sites on multilayer surface of the composites, and the adsorption energy exponentially decreases upon MB adsorption onto the active sites. Similar adsorption process of MB on other physically and chemically modified agricultural waste have also been reported [59, 60]. In this sense, it is conceivable that the positively charged synthetic dye diffused, interacted, occupied the active sites on the surface of PAT composites, and stabilized most likely by the electronegative functional groups and TiO$_2$ NPs via intermolecular hydrogen bonding and electrostatic attractions.

As the Freundlich isotherm model does not provide the maximum adsorption capacity (Q_m), those of MB onto the PAT composites were then deduced from the best fit of Langmuir isotherm model. The Q_m values of MB on PAT$^{(0)}$ and PAT$^{(0.005)}$ were estimated to be 435 and 571 mg g^{-1}, respectively, highlighting enhanced adsorptive removal
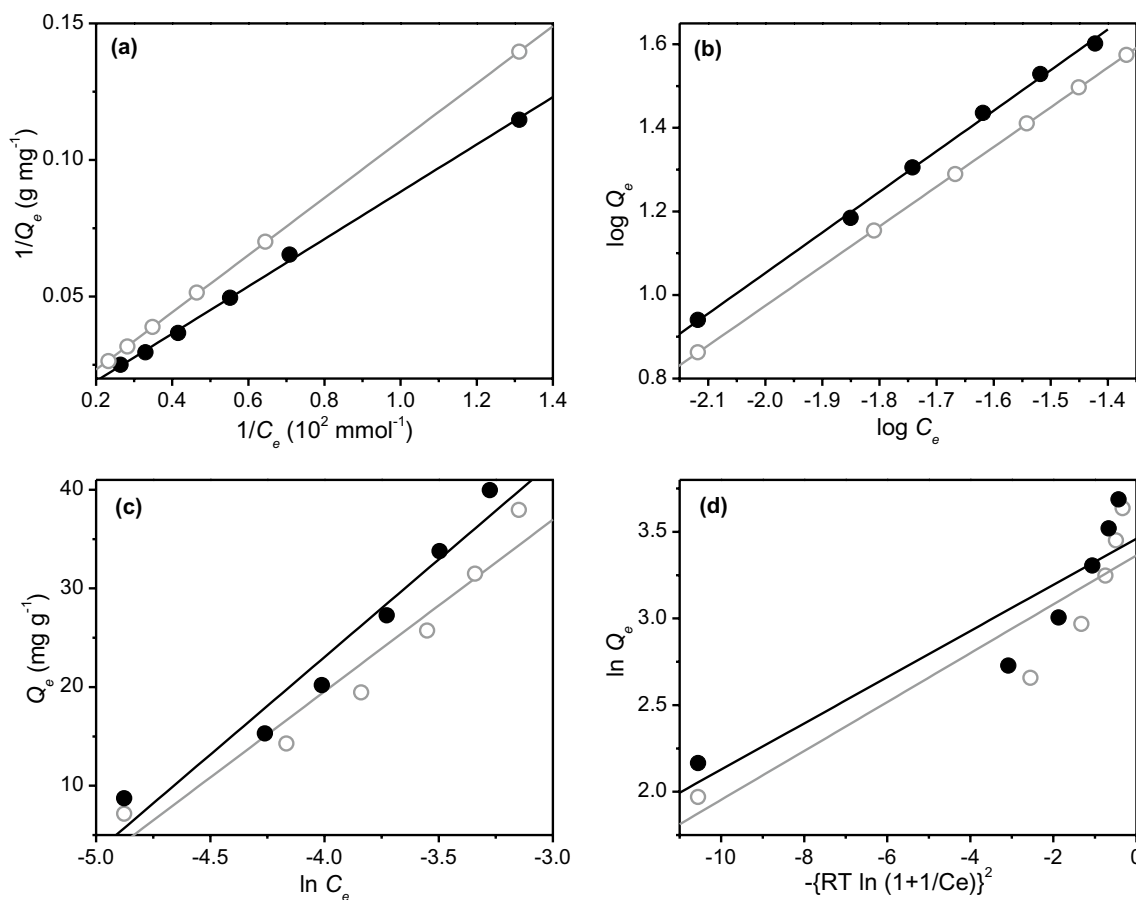

Fig. 9 The adsorption isotherm data of MB on PAT$^{(0)}$ (Circle) and PAT$^{(0.005)}$ (Filled circle) fitted with **a** Langmuir, **b** Freundlich, **c** Temkin, and **d** Dubinin–Radushkevich isotherm models. The grey and black solid lines are the best fits of MB adsorption data on PAT$^{(0)}$ and PAT$^{(0.005)}$
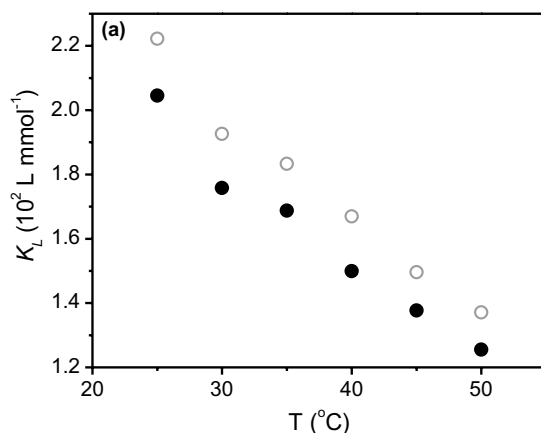
Table 2 The empirical two-parameter isotherm models applied for the adsorption of MB on $PAT^{(0)}$ and $PAT^{(0.005)}$ and their parameters deduced from the best fitting on the experimental data

Isotherm model	Parameters	$PAT^{(0)}$	$PAT^{(0.005)}$
Langmuir			
	$Q_m(mg\ g^{-1})$	435	571
	$K_L(L\ mmol^{-1})$	0.022	0.020
	R^2	0.999	0.999
	χ^2	<0.001	<0.001
Freundlich			
	K_F	649	989
	n	1.053	1.029
	R^2	0.999	0.999
	χ^2	<0.001	<0.001
Temkin			
	$K_T(L\ mmol^{-1})$	168	175
	$b_T(kJ\ mol^{-1})$	0.142	0.125
	R^2	0.953	0.956
	χ^2	0.941	7.46
Dubinin–Radushkevich			
	$Q_m(mg\ g^{-1})$	28.9	31.8
	$\beta(J\ mol^{-1})$	0.141	0.133
	R^2	0.838	0.834
	χ^2	0.075	0.065

of MB upon the incorporation of TiO_2 NPs into the PAT composites.

3.4 The effect of temperature

The effect of temperature on the MB adsorption onto the PAT composites provided an insight into the thermodynamics of the adsorption process. Figure 10a shows that, within the range of temperature from 25 to 50 °C, the K_L values decreased nonlinearly with the temperature. This was an indicative of decreasing Q_e and immobilization of MB on the surface of the PAT composites at higher temperature. In this sense, the higher temperature enhanced the mobility of the synthetic dye as well as disrupted the interactions between MB and functional groups of the PAT composites. The decrease in the Q_e value at higher temperature has also been reported in the adsorption of many adsorbates on biosorbents [61, 62].

Based on the K_L values (see Table 2), K_e^0 and ΔG_{ads}^0 were calculated using Eq. (11 and 12), respectively. The ΔG_{ads}^0 of MB adsorption on $PAT^{(0)}$ and $PAT^{(0.005)}$ at room temperature was estimated to be – 25.1 and – 24.9 kJ mol^{-1}, indicating that the adsorption process was spontaneous. The plot of ΔG_{ads}^0 values against temperature, T, is shown in Fig. 10b. The ΔH^o value which was deduced from the y-intercept of the linear regression plot was found to be – 15.12 and – 15.24 kJ mol^{-1} for MB adsorption on $PAT^{(0)}$ and $PAT^{(0.005)}$, respectively, whereas ΔS^o value was estimated from the slope of the plot to be 0.033 and 0.032 kJ mol^{-1} K^{-1}. Overall thermodynamics parameters suggested that the adsorption of MB on the PAT composites was exothermic as a certain amount of energy was released from the adsorption, and the adsorption increased the concentration of the dye and irregularity on the interface and inside the adsorbents [63].

3.5 The effect of TiO_2 NPs loading content

The adsorption was basically believed to be governed by the surface area and pore size of the adsorbents composite. In this study, the adsorptive removal of MB using the PAT composites with different loading contents of TiO_2 NPs was evaluated at the same experimental conditions. The
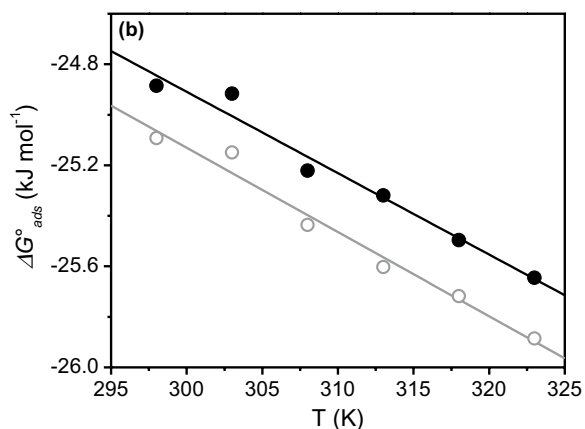

Fig. 10 **a** The plots of K_L of MB adsorption on $PAT^{(0)}$ (Circle) and $PAT^{(0.005)}$ (Filled circle) as a function of temperature (25–50 °C), and **b** the plot of ΔG_{ads}^0 as a function of T from which the thermodynamics parameters were estimated. The grey and black solid lines are the best fits of MB adsorption data on $PAT^{(0)}$ and $PAT^{(0.005)}$

BET surface area was found to be within 2.31–13.5 $m^2 g^{-1}$, while the BJH pore volume was in the range of 0.008–0.053 $cm^3 g^{-1}$. As presented in Fig. 11a, the surface area and pore size increased with the TiO_2 NPs content in the PAT composites, suggesting strongly that the TiO_2 NPs might contribute not only on the surface characteristics, but also on the surface area and the adsorptive capability of the PAT composites. The latter was revealed by the increase in the Q_m value of MB adsorption onto PAT composites with TiO_2 NPs content, where it was estimated based on Langmuir isotherm model to be 467, 571, 637, and 601 $mg g^{-1}$ for PAT$^{(0)}$, PAT$^{(0.005)}$, PAT$^{(0.05)}$, and PAT$^{(0.25)}$, respectively, as shown in Fig. 11b.

The high Q_m value of MB implied the efficient adsorption of the positively charged synthetic dye onto the PAT composites. It can be attributed to the negatively net surface charge of the PAT composites, due to the formation of carboxylate anions of pectin and alginate at ambient pH, as proven by their pH_{pzc} being 4.27−4.48 (see Fig. 4). Upon incorporation of TiO_2 NPs, the net surface charge was almost unchanged, indicating that the formation of the total carboxylate anions remained unaffected. In fact, the incorporation of TiO_2 NPs modified the structure of the pectin-alginate matrix, increasing the surface area of the PAT composites in such a way that more functional groups, especially the carboxylates, of the pectin and alginate were exposed to interact with the synthetic dye. Thus, it is conceivable that MB is attracted more easily by the electrostatic interactions on the active sites and it is then stabilized by the functional groups on the surface of PAT composites with higher TiO_2 NPs content.

The efficient adsorptive removal of MB using the PAT composites was compared with other potential reported adsorbents in Table 3. The Q_m values of MB were generally high on calcium alginate membrane [64], activated carbon [65], calcium alginate beads [65], graphene oxide-sodium alginate composite [66], reduced graphene oxide-TiO_2 NPs composites [67], microwave modified nano-silica beads [68], and agar-graphene oxide composites [63]. The Q_m values of MB on PAT composites in this study were lower than those adsorbents, but they were at least comparable with those on nano-silica beads [68] and were superior compared to most reported biopolymers and their composites (such as pectin gel microsphere [69], cellulose composite [73], chitosan-sepiolite composite [77], magnetite-pectin

composite [71], and magnetite-silica-pectin composite [71]), clays-based materials (clay-biochar [77], zeolite [78], red kaolin [70], kaolin [78], chitosan modified zeolite [77]), and agro-wastes (modified rice husk [68] and date palm leaves [76]).

Table 3 A comparison of Q_m values of various types of adsorbents in the removal of MB from aqueous solution

| Adsorbent	Q_m(mg g^{-1})	References
Calcium alginate membrane	3056	[64]
Activated carbon	1030	[65]
Graphene oxide sodium alginate gels	833	[66]
Calcium alginate beads	800	[65]
Reduced graphene oxide-TiO_2 composites	685–848	[67]
Microwave modified nano-silica	680	[68]
Agar/graphene oxide composite	532–578	[63]
Nano-silica beads	548	[68]
Pectin gel microsphere	285	[69]
Red kaolin	240	[70]
Magnetite-silica-pectin composite	179	[71]
chitosanepichlorohydrin/zeolite	156	[72]
Magnetite-pectin composite	125	[71]
Polyvinyl alcohol-cellulose-graphene oxide	89	[73]
Polyvinyl alcohol-carboxymethyl cellulose	83	[73]
Microwave assisted corncob activated carbon	82.7	[74]
Strychnos potatorum seeds	78.8	[75]
Modified rice husk	65	[68]
Date palm leaves powder	43–58	[76]
Chitosan-sepiolite composite	41	[77]
Chitosan modified zeolite	37	[77]
Kaolin	14	[78]
Clay-biochar	12	[77]
Zeolite	9	[78]
Date palm leaves powder	43–58	[76]
PAT$^{(0)}$	435	This work
PAT$^{(0.005)}$	571	This work
PAT$^{(0.05)}$	637	This work
PAT$^{(0.25)}$	601	This work
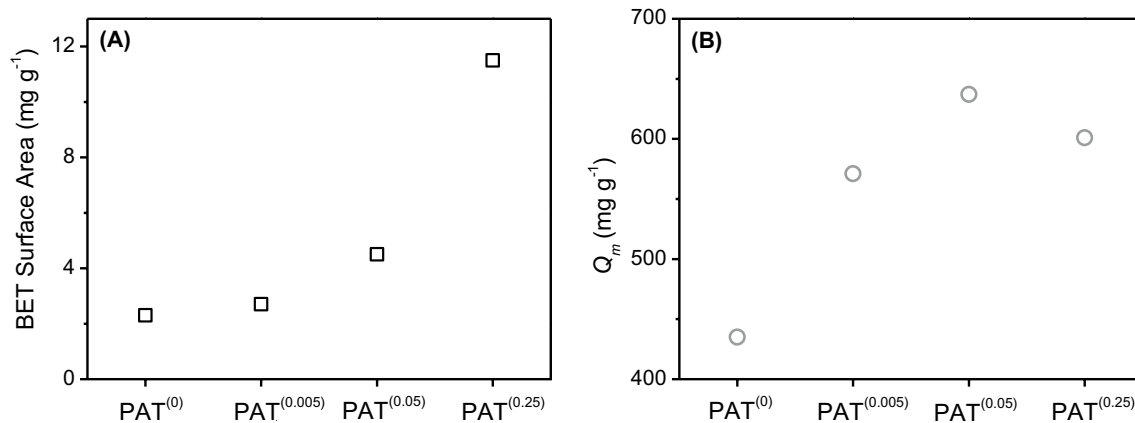
Fig. 11 **a** The plots of BET surface area, and **b** the maximum adsorption capacity (Q_m) obtained from the best fit of Langmuir isotherm model on the adsorption of MB molecules on PAT composites with different TiO_2 NPs loading contents

4 Conclusion

The pectin-alginate-TiO_2 NPs (PAT) composites with different loading contents of TiO_2 NPs were prepared by precipitation method and their structure were characterized by spectroscopic and microscopic methods. Pectin, alginate, and TiO_2 NPs were apparently blended and interconnected by electrostatic and hydrogen bonding interactions in the PAT composites without changing their chemical structure. The adsorptive removal of methylene blue (MB) from aqueous solution as a model of wastewater polluted with synthetic dyes onto the PAT composites was investigated. The maximum adsorption capacity (Q_m) of MB was in the range of 435–637 mg g^{-1}, increasing with the TiO_2 NPs loading content. The adsorption capacity enhanced with the incorporation of TiO_2 NPs into the PAT composites due to the increase of the BET surface area, promoting more interactions between (i) the functional groups of pectin and alginate with the synthetic dye and (ii) electron-deficient heterocyclic aromatic rings of MB with the electron-rich Ti atoms on the surface of the NPs. The adsorption of MB on the surface of the PAT composites followed the Freundlich isotherm model, suggesting the surface heterogeneity of the PAT composites and that adsorption of the synthetic dye occurred on active sites on multilayer surface of the composites. The adsorption kinetics was pseudo-second order, governed by two intraparticle diffusion behaviors, i.e. the fast external diffusion at early times of contact time, followed by slower diffusion at the equilibrium phase at the contact time longer 15 min. The MB adsorption onto the PAT composites was controlled by rate-limiting process of both the intraparticle and film diffusion.

The thermodynamic parameters, including Gibbs free energy, enthalpy, and entropy, deduced from the effect of temperature on the adsorption suggested that the process was exothermic, spontaneous, and an increase in irregularity on the surface and inside of the PAT composites. The maximum adsorption capacity of MB molecules on the PAT composites were generally lower than that on activated carbon, calcium alginate membrane, and graphene oxide based composites, but it was comparable or much higher than those on many biopolymers and their composites, clay-based materials, chemically treated minerals, and agrowastes. Overall results indicated that PAT composites are promising to be utilized as an adsorbent in wastewater treatment to remove the synthetic dyes efficiently. This study also provided an insight into the adsorption mechanism of the synthetic dyes onto the biopolymers-titania composites which might be also useful to understand the efficient degradation of the adsorbed dyes due to the photocatalytic activity of the TiO_2 NPs under UV light irradiation.

Author contributions All of authors had made contributions to this paper. NIIZ carried out the adsorption experiments, SLNZ and NZAD involved in the sample processing, AHM, EK contributed in sample characterizations, and AU conceptualized, supervised the experiments, interpreted the data, and wrote the manuscript.

Compliance with ethical standards

Conflicts of interest There are no conflicts of interest to declare.

References

1. Hunger K (ed) (2003) Industrial dyes; chemistry, properties, applications. Wiley-VCH, Germany

2. Sivakumar D, Parthiban R, Senthil Kumar P, Saravanan A (2020) Synthesis and characterization of ultrasonic-assisted *Delonix regia* seeds: modelling and application in dye adsorption. Desalin Water Treat 173:427–441

3. Kant R (2012) Textile dyeing industry an environmental hazard. Nat Sci 4:22–26

4. Chequer FMD, de Oliveira GAR, Ferraz ERA, Cardoso JC, Zanoni MVB, de Oliveira DP (2013) Textile dyes: dyeing process and environmental impact. In: Gunay M (ed) Eco-friendly textile dyeing and finishing. IntechOpen, London, pp 151–176

5. Lellis B, Fávaro-Polonio CZ, Pamphile JA, Polonio JC (2019) Effects of textile dyes on health and the environment and bioremediation potential of living organisms. Biotechnol Res Innov 3:275–290

6. Pereira L, Alves M (2012) Dyes—environmental impact and remediation environmental protection strategies for sustainable development. In: Malik A, Grohmann E (eds) environmental protection strategies for sustainable development. Springer, Berlin, pp 111–162

7. Markandeya M, Shukla SP, Mohan D (2017) Toxicity of disperse dyes and its removal from wastewater using various adsorbents: a review. Res J Environ Toxicol 11:72–89

8. Sadegh H, Mazloumbilandi M, Chahardouri M (2017) Low-cost materials with adsorption performance. In: Martínez L, Kharissova O, Kharisov B (eds) Handbook of ecomaterials. Springer, Cham, pp 1–33

9. Bhatia D, Sharma NR, Singh J, Kanwar RS (2017) Biological methods for textile dye removal from wastewater: a review. Crit Rev Environ Sci Technol 10:1–41

10. Piaskowski K, Świderska-Dąbrowska R, Zarzycki PK (2018) Dye removal from water and wastewater using various physical, chemical, and biological processes. J AOAC Int 1010:1371–1384

11. Jeevanantham S, Saravanan A, Hemavathy RV, Kumar PS, Yaashikaa PR, Yuvaraj D (2019) Removal of toxic pollutants from water environment by phytoremediation: a survey on application and future prospects. Environ Technol Innov 13:264–276

12. Değermenci GD, Değermenci N, Ayvaoğlu V, Durmaz E, Çakir D, Akan E (2019) Adsorption of reactive dyes on lignocellulosic waste; characterization, equilibrium, kinetic and thermodynamic studies. J Clean Prod 225:1220–1229

13. Saravanan A, Kumar PS, Yashwanthraj M (2017) Sequestration of toxic CVI) ions from industrial wastewater using waste biomass: a review. Desalin Water Treat 68:245–266

14. Pavithra KG, Kumar PS, Jaikumar V, Rajan PS (2019) Removal of colorants from wastewater: a review on sources and treatment strategies. J Ind Eng Chem 75:1–19

15. Kumar PS, Joshiba GJ, Femina CC, Varshini P, Priyadharshini S, Karthick MSA, Jothirani R (2019) A critical review on recent developments in the low-cost adsorption of dyes from wastewater. Desalin Water Treat 172:395–416

16. Saravanan A, Karishma S, Jeevanantham S, Jeyasri S, Kiruthika AR, Kumar PS, Yaashikaa PR (2020) Optimization and modeling of reactive yellow adsorption by surface modified Delonix regia seed: study of nonlinear isotherm and kinetic parameters. Surf Interfaces 20:100520

17. Mohammed MA, Shitu A, Ibrahim A (2014) Removal of methylene blue using low cost adsorbent: a review. Res J Chem Sci 4:91–103

18. Sulyman M, Namiesnik J, Gierak A (2017) Low-cost adsorbents derived from agricultural by-products/wastes for enhancing contaminant uptakes from wastewater: a review. Pol J Environ Stud 26:479–510

19. Suganya S, Kumar PS (2018) Kinetic and thermodynamic analysis for the redemption of effluents containing Solochrome Black T onto Powdered activated carbon: a validation of new Solid-Liquid phase equilibrium model. J Mol Liq 259:88–101

20. Anitha T, Kumar PS, Kumar KS (2016) Synthesis of nano-sized chitosan blended polyvinyl alcohol for theremoval of Eosin Yellow dye from aqueous solution. J Water Process Eng 13:127–136

21. Abdulhameed AS, Mohammad AKT, Jawad AH (2019) Application of response surface methodology for enhanced synthesis of chitosan tripolyphosphate/TiO2 nanocomposite and adsorption of reactive orange 16 dye. J Clean Prod 232:43–56

22. Mohammed IA, Jawad AH, Abdulhameed AS, Mastuli MS (2020) Physicochemical modification of chitosan with fly ash and tripolyphosphate for removal of reactive red 120 dye: statistical optimization and mechanism study. Int J Biol Macromol 161:503–513

23. Abdulhameed AS, Mohammad AKT, Jawad AH (2019) Modeling and mechanism of reactive orange 16 dye adsorption by chitosan-glyoxal/TiO$_2$ nanocomposite: application of response surface methodology. Desalin Water Treat 164:346–360

24. Jawad AH, Abdulhameed AS, Mastuli MS (2020) Mesoporous crosslinked chitosan-activated charcoal composite for the removal of thionine cationic dye: comprehensive adsorption and mechanism study. J Polym Environ 28:1095–1105

25. Jawad AH, Malek NNA, Abdulhameed AS, Razuan R (2020) Synthesis of magnetic chitosan-fly ash/Fe$_3$O$_4$ composite for adsorption of reactive orange 16 dye: optimization by Box-Behnken design. J Polym Environ 28:1068–1082

26. Malek NNA, Jawad AH, Abdulhameed AS, Ismail K, Hameed BH (2020) New magnetic Schiff's base-chitosan-glyoxal/fly ash/Fe3O4 biocomposite for the removal of anionic azo dye: an optimized process. Int J Biol Macromol 146:530–539

27. Renita AA, Kumar PS, Jabasingh SA (2019) Redemption of acid fuchsin dye from wastewater using de-oiled biomass: kinetics and isotherm analysis. Bioresour Technol Rep 7:100300

28. Kumar SP, Subramaniam R (2013) Process optimization studies of Congo red dye adsorption onto cashew nut shell using response surface methodology. Int J Ind Chem 4:17

29. Premkumar MP, Kumar VV, Kumar PS, Baskaralingam P, Sathyaselvabala V, Vidhyadevi T, Sivanesan S (2013) Kinetic and equilibrium studies on the biosorption of textile dyes onto Plantago ovata seeds. Korean J Chem Eng 30:1248–1256

30. Wang JL, Xu LJ (2012) Advanced oxidation processes for wastewater treatment: Formation of hydroxyl radical and application. Crit Rev Environ Sci Technol 42:251–325

31. Deng Y, Zhao RZ (2015) Advanced oxidation processes (AOPs) in wastewater treatment. Curr Pollut Rep 1:167–176

32. Luttrell T, Halpegamage S, Tao J, Kramer A, Sutter E, Batzill M (2015) Why is anatase a better photocatalyst than rutile? Model studies on epitaxial TiO$_2$ films. Sci Rep 4:4043

33. Zulmajdi SLN, Zamri NII, Yasin HM, Kusrini E, Hobley J, Usman A (2020) Comparative study on the adsorption, kinetics, and thermodynamics of the photocatalytic degradation of six different

synthetic dyes on TiO$_2$ nanoparticles. React Kinet Mech Catal 129:519–534

34. Saikia J, Gogoi A, Baruah S (2019) Nanotechnology for water remediataion. In: Dasgupta N, Ranjan S, Lightfouse E (eds) Environemtnal nanotechnology, vol 2. Springer Nature AG, Switzerland, pp 195–213

35. Janus M, Kusiak-Nejman E, Morawski AW (2011) Determination of the photocatalytic activity of TiO$_2$ with high adsorption capacity. React Kinet Mech Catal 103:279–288

36. Sangareswari M, Sundaram MM (2017) Development of efficiency improved polymer-modified TiO$_2$ for the photocatalytic degradation of an organic dye from wastewater environment. Appl Water Sci 7:1781–1790

37. Chakraborty S, Chowdhury S, Saha PD (2011) Adsorption of crystal violet from aqueous solution onto NaOH-modified rice husk. Carbohydr Polym 86:1533–1541

38. Ratna R, Padhi BS (2012) Pollution due to synthetic dyes toxicity and carcinogenicity studies and remediation. Int J Environ Sci 3:940–955

39. Daud NZA, Said BNM, Ja'afar F, Yasin HM, Kusrini E, Usman A (2019) pH-dependent yield and physicochemical properties of pectin isolated from Citrus maxima. Chem Eng 10:1131–1139

40. Biswal T, Barik B, Sahoo PK (2016) Synthesis and characterization of magnetite-pectin-alginate hybrid bionanocomposite. J Mater Sci Nanotechnol 4:2–8

41. Simonin JP (2016) On the comparison of pseudo-first order and pseudo-second order rate laws in the modeling of adsorption kinetics. Chem Eng J 300:254–263

42. Robati D (2013) Pseudo-second-order kinetic equations for modeling adsorption systems for removal of lead ions using multi-walled carbon nanotube. J Nanostruct Chem 3:55

43. Ho YS, Ng JCY, McKay G (2000) Kinetics of pollutant sorption by biosorbents: review. Sep Purif Methods 29:189–232

44. Viegas RMC, Campinas M, Costa H, Rosa MJ (2014) How do the HSDM and Boyd's model compare for estimating intraparticle diffusion coefficients in adsorption processes. Adsorption 20:737–746

45. Ghaffari HR, Pasalari H, Tajvar AH, Dindarloo K, Goudarzi B, Alipour V, Ghanbarneajd A (2017) Linear and nonlinear two-parameter adsorption isotherm modeling: a case-study. Int J Eng Sci 6:1–11

46. Liu Y, Liu YJ (2008) Biosorption isotherms, kinetics and thermodynamics. Sep Purif Technol 61:229–242

47. Lima EC, Hosseini-Bandegharaei A, Moreno-Piraján JC, Anastopoulos I (2019) A critical review of the estimation of the thermodynamic parameters on adsorption equilibria. Wrong use of equilibrium constant in the Van't Hoof equation for calculation of thermodynamic parameters of adsorption. J Mol Liq 273:425–434

48. Bichara LC, Alvarez PE, Fiori Bimbi MV, Vaca H, Gervasi C, Brandán SA (2016) Structural and spectroscopic study of a pectin isolated from citrus peel by using FTIR and FT-Raman spectra and DFT calculations. Infrared Phys Technol 76:315–327

49. Daemi H, Barikani M (2012) Synthesis and characterization of calcium alginate nanoparticles, sodium homopolymannuronate salt and its calcium nanoparticles. Sci Iranica F Nanotechnol 19:2023–2028

50. Synytsya A, Čopíková J, Matějka P, Machovič V (2003) Fourier transform Raman and infrared spectroscopy of pectins. Carbohydr Polym 54:97–106

51. Mishra RK, Datt M, Pal K, Banthia AK (2008) Preparation and characterization of amidated pectin based hydrogels for drug delivery system. J Mater Sci Mater Med 19:2275–2280

52. Kumar A, Chauhan GS (2010) Extraction and characterization of pectin from apple pomace and its evaluation as lipase (steapsin) inhibitor. Carbohydr Polym 82:454–459

53. Jana S, Trivedi MK, Tallapragada RM, Branton A, Trivedi D, Nayak G, Mishra RK (2015) Characterization of physicochemical and thermal properties of chitosan and sodium alginate after biofield treatment. Pharm Anal Acta 6:1000430

54. Sakurai K, Mizusawa M (2010) X-ray diffraction imaging of anatase and rutile. Anal Chem 82:3519–3522

55. Kumar PS, Sivaranjanee R, Vinothini U, Raghavi M, Rajasekar K, Ramakrishnan K (2013) Adsorption of dye onto raw and surface modified tamarind seeds: isotherms, process design, kinetics and mechanism. Desalin Water Treat 52:2620–2633

56. Kumar PS, Abhinaya RV, Lashmi KG, Arthi V, Pavithra R, Sathyaselvabala V, Kirupha SD, Sivanesan S (2011) Adsorption of methylene blue dye from aqueous solution by agricultural waste: equilibrium, thermodynamics, kinetics, mechanism and process design. Colloid J 73:651–661

57. El-Khaiary MI, Malash GF (2011) Common data analysis errors in batch adsorption studies. Hydrometallurgy 105:314–320

58. Dotto GL, Pinto LAA (2012) Analysis of mass transfer kinetics in the biosorption of synthetic dyes onto Spirulina platensis nanoparticles. Biochem Eng J 68:85–90

59. Suganya S, Kumar PS, Saravanan A, Rajan PS, Ravikumar C (2017) Computation of adsorption parameters for the removal of dye from wastewater by microwave assisted sawdust: theoretical and experimental analysis. Environ Toxicol Pharmacol 50:45–57

60. Manikandan G, Kumar PS, Saravanan A (2018) Modelling and analysis on the removal of methylene blue dye from aqueous solution using physically/chemically modified Ceiba pentandra seeds. J Ind Eng Chem 62:446–461

61. Kusrini E, Usman A, Sani FA, Wilson LD, Abdullah MAA (2019) Simultaneous adsorption of lanthanum and yttrium from aqueous solution by durian rind biosorbent. Environ Monit Assess 191:488

62. Kusrini E, Paramesti SN, Zulys A, Daud NZA, Usman A, Wilson LD, Sofyan N (2019) Kinetics, isotherm, thermodynamic and bioperformance of defluoridation of water using praseodymium-modified chitosan. J Environ Chem Eng 7:103498

63. Chen L, Li Y, Du Q, Wang Z, Xia Y, Yedinak E, Lou J, Ci L (2017) High performance agar/graphene oxide composite aerogel for methylene blue removal. Carbohydr Polym 155:345–353

64. Li Q, Li Y, Ma X, Du Q, Sui K, Wang D, Wang C, Li H, Xia Y (2017) Filtration and adsorption properties of porous calcium alginate membrane for methylene blue removal from water. Chem Eng J 316:623–630

65. Hassan AF, Abdel-Mohsen M, Fouda MMG (2014) Comparative study of calcium alginate, activated carbon, and their composite beads on methylene blue adsorption. Carbohydr Polym 102:192–198

66. Ma T, Chang PR, Zheng P, Zhao F, Ma X (2014) Fabrication of ultra-light graphene-based gels and their adsorption of methylene blue. Chem Eng J 240:595–600

67. Wang H, Gao H, Chen M, Xu X, Wang X, Pan C, Gao J (2016) Microwave-assisted synthesis of reduced graphene oxide/titania nanocomposites as an adsorbent for methylene blue adsorption. Appl Surf Sci 360:840–848

68. Peres EC, Slaviero JC, Cunha AM, Hosseini-Bandegharaei A, Dotto GL (2018) Microwave synthesis of silica nanoparticles and its application for methylene blue adsorption. J Environ Chem Eng 6:649–659

69. Yu LL, Jiang LN, Wang SY, Sun MM, Li DQ, Du GM (2017) Pectin microgel particles as high adsorption rate material for methylene blue: Performance, equilibrium, kinetic, mechanism and regeneration studies. Int J Biol Macromol 112:383–389

70. Jawad AH, Abdulhameed AS (2020) Mesoporous Iraqi red kaolin clay as an efficient adsorbent for methylene blue dye: adsorption kinetic, isotherm and mechanism study. Surf Interface 18:100422

71. Attallah OA, Al-ghobashy MA, Nabsen M, Salem MY (2016) Solution with magnetite/pectin and magnetite/isotherm and mechanism analysis. RSC Adv 6:11461–11480

72. Jawad AH, Abdulhameed AS, Abdallah R, Yaseen ZM (2020) Zwitterion composite chitosan-epichlorohydrin/zeolite for adsorption of methylene blue and reactive red 120 dyes. Int J Biol Macromol 163:756–765

73. Dai H, Huang Y, Huang H (2018) Eco-friendly polyvinyl alcohol/carboxymethyl cellulose hydrogels reinforced with graphene oxide and bentonite for enhanced adsorption of methylene blue. Carbohydr Polym 185:1–11

74. Tharaneedhar V, Kumar PS, Saravanan A, Ravikumar C, Jaikumar V (2017) Prediction and interpretation of adsorption parameters for the sequestration of methylene blue dye from aqueous solution using microwave assisted corncob activated carbon. Sustain Mater Technol 11:1–11

75. Senthamarai C, Kumar PS, Priyadharshini M, Vijayalakshmi P, Kumar VV, Baskaralingam P, Thiruvengadaravi KV, Sivanesan S (2013) Adsorption behavior of methylene blue dye onto surface modified strychnos potatorum seeds. Environ Prog Sustain Energy 32:624–632

76. Gouamid M, Ouahrani MR, Bensaci MB (2013) Adsorption equilibrium, kinetics and thermodynamics of methylene blue from aqueous solutions using date palm leaves. Energy Proc 36:898–907

77. Marrakchi F, Khanday WA, Asif M, Hameed BH (2016) Cross-linked chitosan/sepiolite composite for the adsorption of methylene blue and reactive orange 16. Int J Biol Macromol 93:1231–1239

78. Rida K, Bouraoui S, Hadnine S (2013) Adsorption of methylene blue from aqueous solution by kaolin and zeolite. Appl Clay Sci 83–84:99–105